Molecular structure and infrared spectra of dimethyl fumarate†

Susy Lopes,[a] **Leszek Lapinski**[ab] **and Rui Fausto**[*a]

[a] *Department of Chemistry (CQC), University of Coimbra, P-3004-535, Coimbra, Portugal.*
 E-mail: rfausto@ci.uc.pt
[b] *Institute of Physics, Polish Academy of Sciences, PL-02-668, Warsaw, Poland*

Infrared spectra of dimethyl fumarate isolated in low-temperature argon and xenon matrixes and of the compound in the solid amorphous and crystalline states have been studied. Theoretical calculations, carried out at the MP2/6-31G** and DFT(B3LYP)/6-31G** levels, predict three planar conformers of low internal energy, all of them exhibiting the methyl ester moieties in the *cis* (C–O) configuration: the conformational ground state (conformer **I**), with the two O=C–C=C dihedrals equal to 0°, and forms **II** and **III**, where one or both O=C–C=C dihedrals are 180°. In the spectra of the matrix isolated compound, characteristic bands of all three conformers were identified. During annealing of the xenon matrix up to 60 K, conversion of the less stable conformers, **II** and **III**, into the most stable conformer, **I**, was observed. In the amorphous solid, these three conformers could also be identified spectroscopically. The IR and Raman spectra of the crystalline phase clearly show that in the crystal only form **I** is present, since no bands ascribable to other conformers could be observed.

Introduction

Dimethyl fumarate ($CH_3OOCCH=CHCOOCH_3$, DMFU) is the *E* isomer of butenedioic acid dimethyl ester. At room temperature, the compound is solid (triclinic crystals).[1] DMFU is commonly used in food industry as an antifungal agent[2–4] and in medicine in the treatment of psoriasis.[5] It also has applications in the polymer industry.[6,7]

From a structural point of view, DMFU consists of two ester groups attached to the opposite sides of the C=C double bond of the ethylene fragment (Fig. 1). As is usually the case in non-sterically constrained carboxylic esters,[8–11] the methyl ester groups adopt preferentially the *cis* (C–O) configuration (CH_3–O–C=O angle equal to 0°), with one of the methyl hydrogen atoms occupying the anti-periplanar orientation relative to the carbonyl group [H–C–O–(C=O) angle equal to 180°]. The energy barrier for interconversion between the low energy *cis* isomers of carboxylic esters, by rotation of the ester group, towards a *trans* orientation (C–O–C=O angle equal to 180°) is well known to be high (30–50 kJ mol⁻¹), and, in general, these latter conformers are not observed experimentally since the *trans*–*cis* energy difference is usually larger than 20 kJ mol⁻¹.[8–11]

In principle, both ester units in DMFU can adopt *cis* or *trans* orientations with respect to the C=C double bond (O=C–C=C dihedral angle equals to 0° and 180°, respectively). The two ester groups are separated quite well in space, so, to a fair approximation, the energy changes corresponding to the rotation of one ester group and then the other can be expected to be additive. Indeed, this was observed previously for the corresponding dicarboxylic acid, (*E*)-butenedioic acid (fumaric acid, HOOCCH=CHCOOH), where the three non-equivalent-by-symmetry conformers differing by internal rotation around the C–C bonds are separated in energy by approximately equal gaps (2–3 kJ mol⁻¹), the *cis*–*cis* conformer being the lowest

energy form, and the *trans*–*trans* the highest.[8] Similar results have also been obtained for other related compounds, such as acrylic and (*E*)-crotonic acids and methyl acrylate.[9–11] The interactions stabilizing, in such α,β-unsaturated carbonyl compounds, the *cis* conformation around the C–C bonds, with respect to the *trans* structures, are weak in nature.[8–11] Hence, the energy differences between *cis* and *trans* conformers are
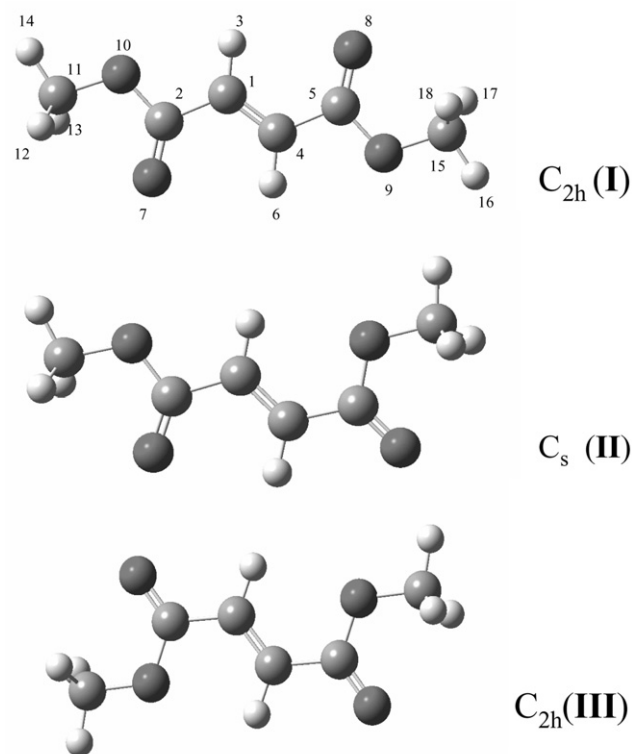
**Fig. 1** Structure of the most stable conformers of DMFU and atom numbering scheme.

---

† Electronic supplementary information (ESI) available: Definition of internal symmetry coordinates, calculated frequencies, IR intensities, Raman activities, potential energy distributions and optimized conformers **I**, **II** and **III**. See http://www.rsc.org/suppdata/cp/b2/b203246p/

relatively small and, in general, more than one conformer can be observed experimentally.[8–11]

The IR and Raman spectra of DMFU have been reported in the past. Téllez *et al.*[12] interpreted the spectra on the basis of co-existence of two conformers: *trans–trans* and *trans–cis*. The spectra were recorded in the temperature range 12–390 K in the solid, liquid and vapour phases as well as in solution in CCl_4. The *trans–trans* conformer (C_{2h} molecular symmetry) was postulated to be the one present in the solid state. In the liquid phase (molten samples or solutions in CCl_4) and in the vapour phase additional infrared and Raman bands were observed and interpreted as due to the presence of a second conformer (the *trans–cis* conformer, of C_s molecular symmetry). Compton *et al.*[13] also reported the vibrational spectra of several fumarates and maleates in the liquid and solid states, at various temperatures, along with their assignments to the conformers. Several errors were made by these authors, such as the incorrect statement of the selection rules for the *trans–trans* conformer and the assignment of Raman bands to A_u and B_u modes, while some of the depolarization measurements also appear to be incorrect.

In the present work the conformational equilibria of DMFU were studied by theoretical methods of quantum chemistry and by experimental Raman and IR spectroscopy, including low temperature matrix-isolation spectroscopy. Identification and structural characterization of possible conformers of DMFU are important both from a fundamental perspective and practical use of this molecule, since it is well known that the macroscopic properties of a substance are strongly dependent on its conformational equilibrium. As described in detail below, the theoretical calculations predicted three planar conformers of low internal energy (*cis–cis*, *cis–trans* and *trans–trans*; see Fig. 1). All other possible structures are higher in energy by more than 30 kJ mol^{-1} and are not of practical importance. The assignment of observed IR and Raman bands was then based on comparison with the spectra theoretically predicted at DFT(B3LYP)/6-31G** level for the three low energy forms of the compound, whose simultaneous presence in the low temperature matrixes could be unequivocally established for the first time.

Experimental

Dimethyl fumarate used in the present study was prepared by acid-catalyzed esterification of fumaric acid.

The sample of DMFU was placed in a glass tube kept at room temperature and the sublimated compound was introduced in the cryostat chamber through a needle valve. The DMFU vapours were deposited together with a large excess of the matrix gas (argon 99.9999%, or xenon 99.995%, both from Air Liquide) onto the cold KBr window ($T = 8$ K) mounted on the cold tip of the APD Cryogenics DE-202A closed-cycle helium refrigerator. Care was taken to keep the guest-to-host ratio in matrixes low enough to avoid association.

The solid amorphous layer of DMFU was prepared in the same manner as the matrixes, but with the flux of the matrix gas cut off. The layer was then allowed to anneal at a slowly increasing temperature, up to 200 K. Infrared spectra were collected during this process every 20 K of temperature change. After the temperature exceeded 200 K, the substrate was cooled back to 8 K and the final spectrum was recorded.

The IR spectra of the matrixes were recorded with a resolution 0.5 cm^{-1}, on a Mattson FTIR spectrometer (Infinity 60 AR). In the case of the solid (amorphous or crystalline) layers the resolution was 1.0 cm^{-1}. A SiC globar source, a KBr beamsplitter and a DTGS mid-IR detector were used in these measurements.

The Raman spectra were obtained using a Spex 1403 double monochromator spectrometer (focal length 0.85 m, aperture *f*/7.8) equipped with holographic gratings with 1800 groove mm^{-1} (reference 1800-1SHD). Radiation of 514.5 nm from an Ar$^+$ laser (Spectra-Physics, model 164-05), adjusted to provide 220 mW power at the sample, was used for excitation. Detection was effected using a thermoelectrically cooled Hamamatsu R928 photomultiplier. The spectrum was recorded using increments of 2 cm^{-1} and integration times of 1 s.

Computational

The geometries of the different conformers of DMFU were optimized at the DFT(B3LYP)/6-31G** level of theory. Subsequently, the harmonic wavenumbers were calculated, at the optimized geometries, using the same theoretical method. Optimized geometries and energies of the three most stable conformers of DMFU were also calculated at the MP2/6-31G** level. All the calculations were carried out using the GAUSSIAN 98 program package.[14]

Transformations of the harmonic force constant matrices in Cartesian coordinates to the molecule-fixed internal coordinates allowed for ordinary normal-coordinate analysis to be performed as described by Schachtschneider.[15] The list of symmetry-adopted internal coordinates used in this analysis is given in the Supplementary Material Table S1† (for the atom numbering see Fig. 1). The complete list of calculated frequencies and intensities are provided in the Supplementary Material Tables S2–S4.† Potential energy distribution (PED) matrices[16] have been calculated and the elements of these matrices greater than 10%, as well as frequencies and intensities of the bands observed in the experimental spectra, are given in Tables 1 and 2. In order to correct for vibrational anharmonicity, basis set truncation and the neglected part of the electron correlation, the calculated DFT wavenumbers were scaled down by a single scale factor of 0.97.

Results and discussion

A theoretical search through the potential energy surface of DMFU has been undertaken. The calculations, carried out at MP2/6-31G** and DFT(B3LYP)/6-31G** levels of theory, predict three low-energy conformers of the compound, each of them corresponding to a structure with coplanar carbon and oxygen atoms (see Fig. 1; for complete calculated optimized geometries see the Supplementary Material Table S5†). Conjugation of the π-electron system along the C=O and C=C double bonds stabilizes the planar structures. According to the calculations, the most stable conformer is of C_{2h} symmetry, with both ester groups in the *cis* orientation with respect to the central C=C bond (*cis–cis* form, from here named conformer **I**). Two weak hydrogen bonds between the carbonyl oxygen atoms and the corresponding β-hydrogen atoms, closing intramolecular five-membered rings, are the main factor responsible for the slight stabilization of conformer **I** with respect to forms **II** (*cis–trans*) and **III** *(trans–trans)*. It shall be noticed that the interaction of β-hydrogen atoms with the lone pair of the carbonyl oxygen can be expected to be more important than with those of the methoxylic ester oxygen, because in the first case the hybridization brings the maximum of electron density in the plane of the molecule and in the second case out of the plane. Indeed, the stabilizing effects of the CH∴O=C and CH∴OR (with R = H or alkyl) interactions have already been compared in detail elsewhere[17,18] and the above assumption clearly confirmed. Rotation of one of the ester groups by 180° leads to conformer **II** (C_s), which is higher in energy by 3.4 kJ mol^{-1} (MP2 + ZPE(DFT)) than the most

Table 1 Observed and calculated [scaled; DFT(B3LYP)/6-31G**] frequencies and intensities for the isolated monomeric forms of DMFU

Approximate description	Observed			Form	Calculated		
	Xe		Ar				
	ν_{exp}/cm^{-1}	$I_{exp}{}^a$	ν_{exp}/cm^{-1}		ν_{calc}/cm^{-1}	I_{calc}	PED
	3459.3	vw	3465.9	I			ν(C=O) asym + ν(C=O) sym
ν(C–H) asym	3080.7	vw		I	3125.6	0.1	ν(C–H) asym (100)
				II	3134.5	0.2	ν(C–H) asym (70), ν(C–H) sym (30)
				III	3139.5	0.3	ν(C–H asym (100)
ν(C–H) sym	3080.7	vw		II	3124.7	0.3	ν(C–H) sym (69), ν(C–H) asym (30)
ν(CH$_3$) asym (2)	3030.2	vw	3044.2	I	3082.6	32.4	ν(CH$_3$) asym (2) (98)
				II	3081.5	11.6	ν(CH$_3$) asym (2)(52), ν(CH$_3$) asym(1)(46)
	3023.6	w	3065.5	III	3082.3	25.8	ν(CH$_3$) asym (2) (98)
ν(CH$_3$) asym (1)	3030.2	vw	3044.2	II	3082.5	18.9	ν(CH$_3$) asym (1)(52), ν(CH$_3$) asym (2) (46)
	3023.6	w	3065.5				
ν(CH$_3$) asym′ (1)	2989.5	w		I	3048.1	36.3	ν(CH$_3$) asym′ (1) (100)
				II	3049.0	19.9	ν(CH$_3$) asym′ (1) (51), ν(CH$_3$) asym′ (2) (49)
ν(CH$_3$) asym′ (2)		w		II	3048.1	18.7	ν(CH$_3$) asym′ (2)(51), ν(CH$_3$) asym′ (1)(49)
				III	3049.3	38.9	ν(CH$_3$) asym′ (2) (100)
ν(CH$_3$) sym (2)	2944.6	m	2962.7	I	2973.2	59.6	ν(CH$_3$) sym (2) (98)
				II	2973.5	22.9	ν(CH$_3$) sym (2)(70), ν(CH$_3$) sym (1)(28)
				III	2973.9	55.6	ν(CH$_3$) sym (2) (98)
ν(CH$_3$) sym (1)	2944.6	m	2962.7	II	2973.7	38.5	ν(CH$_3$) sym (1) (70), ν(CH$_3$) sym (2) (28)
	2900.0	sh	2910.3	I			δ(CH$_3$) asym′ (1) + δ(CH$_3$) asym′ (2)
	2882.4	vw	2845.2	I			δ(CH$_3$) sym (2) + δ(CH$_3$) sym (1)
			1762.5	II			ν(C–O) asym + δ(CH) asym
ν(C=O) asym	1743.9	sh	1744.4	II	1757.7	66.1	ν(C=O) asym (80)
ν(C=O) sym	1739.4	sh	1748.8	II	1749.7	327.1	ν(C=O) sym (87)
ν(C=O) asym				III	1749.9	475.3	ν(C=O) asym (87)
			1741.1				
ν(C=O) asym	1736.1	S	1739.5	I	1747.2	350.0	ν(C=O) asym (88)
	1733.4	sh	1737.8				
	1724.7	m	1734.9				
ν(C=C)	1645.7	w	1652.7	II	1662.4	31.2	ν(C=C) (68), δ(CH) sym (13)
δ(CH$_3$) asym (2)	1455.3	m	1461.6	I	1462.9	13.2	δ(CH$_3$) asym (2)(78), δ(CH$_3$) sym (2)(12)
				II	1464.5	7.5	δ(CH$_3$) asym (2)(39), δ(CH$_3$) asym (1)(39)
				III	1464.4	13.7	δ(CH$_3$) asym (2)(79), δ(CH$_3$) sym (2)(12)
δ(CH$_3$) asym (1)	1455.3	m	1461.6	II	1462.6	8.3	δ(CH$_3$) asym (1)(41), δ(CH$_3$) asym (2)(40)
δCH$_3$ asym′ (1)	1444.2	m		I	1450.5	13.0	δ(CH$_3$) asym′ (1)(94)
				II	1450.9	6.6	δ(CH$_3$) asym′ (1)(47), δ(CH$_3$) asym′ (2)(47)
δ((CH$_3$) asym′ (2)	1444.2	m	1449.5	III	1450.7	13.0	δ(CH$_3$) asym′ (2)(94)
				II	1450.1	6.3	δ(CH$_3$) asym′ (2)(47), δ(CH$_3$) asym′ (1)(47)
δ(CH$_3$) sym (2)	1437.7	S	1441.3	I	1437.3	40.8	δ(CH$_3$) sym (2)(82)
				II	1438.3	25.2	δ(CH$_3$) sym (2)(63), δ(CH$_3$) sym (1)(19)
				III	1437.6	27.9	δ(CH$_3$) sym (2)(83)
δ(CH$_3$) sym (1)	1437.7	S	1441.3	II	1436.0	7.2	δ(CH$_3$) sym (1)(65), δ(CH$_3$) sym (2)(20)
ν(C–C) asym	1307.4	S sh	1308.0	I	1294.6	881.8	δ(CH) asym (33), ν(C–C) asym (24), ν(C–O) asym (22), δ(C=O) asym (12)
	1301.8		1302.5				
	1285.9	m		I			δ(C=O) asym + γ(C=O) asym
				III			
ν(C–C) asym	1278.0	m	1279.4	II	1672.2	493.6	ν(C–O) asym (22), ν(C–C) asym (16), ν(C–O) sym (15), δ(CH) sym (11)
	1272.7	m	1275.5				
δ(CH) sym	1266.3	m	1262.5	II	1252.0	228.7	δ(CH) sym (30), δ(CH) asym (27)
	1261.0	m	1259.1				
ν(C–C) asym	1256.9	m	1255.8	III	1251.4	721.6	ν(C–O) asym (36), δ(CH) asym (21), ν(C–C) asym (19), δ(C=O) asym (15)
δ(CH) asym	1229.3	sh	1228.5	III	1217.9	218.8	δ(CH) asym (64), ν(C–C) asym (15)
	1227.4	m	1226.0				
γ(CH$_3$) asym	1194.5	m	1198.9	II	1184.7	92.8	γ(CH$_3$) asym (44), δ(CH) asym (15)
γ(CH$_3$) asym	1193.1	sh	1196.2	I	1180.1	92.7	γ(CH$_3$) asym (71)
	1191.9	S	1193.5				
γ(CH$_3$) sym	1189.2	w	1191.2	II	1175.8	10.3	γ(CH$_3$) sym (65), γ(CH$_3$) asym (12)
γ(CH$_3$) asym	1187.9	sh	1188.6	III	1173.9	36.0	γ(CH$_3$) asym (73)
δ(CH) asym	1173.7	sh	1174.3	II	1163.3	89.0	δ(CH) asym (34), γ(CH$_3$) asym (21)
	1171.7	m	1171.3				
	1168.9	m	1166.7				
δ(CH) asym	1157.9	sh	1157.9	I	1147.9	322.6	δ(CH) asym (51), ν(C–O) asym (19)
	1154.2	S	1154.9				
	1147.5	w	1154.4				
			1147.5				

Table 1 (continued)

Approximate description	Xe ν_{exp}/cm^{-1}	I_{exp}^{a}	Ar ν_{exp}/cm^{-1}	Form	ν_{calc}/cm^{-1}	I_{calc}	PED
ν(C–O(CH$_3$)) asym	{ 1040.5	sh	{ 1046.3				
	1037.1	m	1040.5	II	1041.5	114.3	ν(C–O(CH$_3$)) asym (55), ν(C–O(CH$_3$)) sym (19)
	1035.2	m	1038.4				
			1036.9				
ν(C–O(CH$_3$)) asym	{ 1033.5	sh	{ 1035.2	III	1036.7	119.3	ν(C–O(CH$_3$)) asym (74), ν(C–C) asym (19)
	1030.9	sh	1033.7				
ν(C–O(CH$_3$)) asym	1021.0	m	1023.9	I	1021.0	57.3	ν(C–O(CH$_3$)) asym (65), ν(C–C) asym (22)
ν(C–O(CH$_3$)) sym	1009.0	vw		II	1010.1	9.40	ν(C–O(CH$_3$)) sym (45), ν(C–O(CH$_3$)) asym (19), ν(C–C) asym (12), ν(C–C) sym (11)
γ(C–H) sym	984.9	m	986.2	{ II	1002.6	31.2	γ(C–H) sym (105)
				III	1004.0	31.3	γ(C–H) sym (106)
γ(C–H) sym	979.9	m	983.7	I	999.7	31.9	γ(C–H) sym (106)
ν(C–C) sym	923.1	w	926.1	II	915.5	11.0	ν(C–O(CH$_3$)) sym (18), ν(C–O) sym (15), ν(C–C) asym (14), ν(C–C) sym (11)
γ(C–H) asym	891.5	w	887.6	II	889.4	0.5	γ(C–H) asym (83), γ(C=O) sym (21)
ν(C–O) asym	{ 891.5	w	{ 887.6	I	880.3	19.5	ν(C–O) asym (36), ν(C–C) asym (21), ν(C–O(CH$_3$)) asym (18)
	885.3	w	884.5				
ν(C–O) asym	875.9	vw	876.2	III	864.5	21.6	ν(C–O) asym (38), ν(C–C) asym (18), ν(C–O(CH$_3$)) asym (15)
ν(C–O) asym	860.3	vw	859.7	II	849.9	8.1	ν(C–O) asym (28), ν(C–O) sym (15), ν(C–O(CH$_3$)) asym (11)
γ(C=O) sym	775.9	m	{ 778.4	{ I	754.0	28.5	γ(C=O) sym (88), τ(C=C) (15)
			777.4	III	754.2	26.6	γ(C=O) sym (90), τ(C=C) (17)
γ(C=O) asym	775.9	m	{ 778.4	II	753.6	27.6	γ(C=O) asym (89), τ(C=C) (16)
			777.4				
δ(C=O) sym	745.3	vw	746.6	II	735.6	1.7	δ(C=O) sym (29), δ(CC=C) sym (19), δ(COC) sym (12)
δ(C=O) asym	672.1	m	670.9	I	660.3	20.9	δ(C=O) asym (52), ν(C–C) asym (23), δ(COC) asym (14)
δ(C=O) asym	668.6	vw	667.3	III	656.4	17.6	δ(C=O) asym (47), ν(C–C) asym (24), δ(COC) asym (14)
δ(C=O) asym	664.7	w	665.6	II	652.9	16.3	δ(C=O) asym (41), ν(C–C) asym (23), δ(COC) asym (14)
δ(CCO) sym	529.9	vw	529.9	II	518.0	2.5	δ(CCO) sym (40), δ(C=O) sym (25), δ(CC=C) asym (17)
δ(CCO) asym	521.2	w	521.2	{ I	510.7	9.7	δ(CCO) asym (49), δ(CC=C) asym (18), δ(C=O) asym (13)
				III	509.4	10.3	δ(CCO) asym (48), δ(CC=C) asym (17), δ(C=O) asym (15)

[a] Intensities are presented in a qualitative way: S strong, m, medium, w, weak, vw, very weak, sh, shoulder.

Table 2 Observed IR and Raman frequencies for the amorphous and crystalline phases of DMFU and calculated frequencies for conformer **I**[a]

Approximate description	Crystal IR	Raman	Amorphous IR	Calculated
	3428.9			δ(C=O) asym + δ(C=O) sym
ν(CH$_3$) asym (2)	{ 3078.3		{ 3079.3	
	3054.5		3061.3	3082.6
ν(C–H) sym		3074.1		3123.1
ν(CH$_3$) asym (1)		3063.0		3082.7
ν(CH$_3$) asym' (1)	3022.8		{ 3031.2	3048.1
			3006.3	
ν(CH$_3$) asym' (2)		3028.1		3048.0
ν(CH$_3$) sym (1)		2976.0		2973.3
ν(CH$_3$) sym (2)	2965.9		2958.6	2973.2
	2853.7		2852.5	δ(CH$_3$) sym (2) + δ(CH$_3$) asym' (2)
		2864.4		$2 \times \delta$(CH$_3$) asym' (1)
		1835.9		$2 \times \nu$(C–C) sym
		1812.7		$2 \times \gamma$(C–H) asym

Table 2 (continued)

| Approximate description | Observed | | | Calculated |
| | Crystal | | Amorphous | |
	IR	Raman	IR	
ν(C=O) sym		1734.0		1755.3
ν(C=O) asym	⎧ 1719.3		1725.8	1747.2
	⎪ 1680.0			
	⎨ 1663.8			
	⎪ 1647.5			
	⎩ 1626.6			
ν(C=C)		⎰ 1692.0		1674.9
		⎱ 1668.2		
ν(C=C) (II)			1646.9	1662.4
δ(CH$_3$) asym (1)		1467.4		1462.8
δ(CH$_3$) asym' (2)		1455.8		1450.5
δ(CH$_3$) asym (2)	⎰ 1455.6		1460.0	1462.9
	⎱ 1445.1			
δ(CH$_3$) asym' (1)	1438.9		1442.7	1450.5
δ(CH$_3$) sym (2)	1428.3			1437.3
δ(CH) sym		⎰ 1322.4		1298.8
		⎱ 1309.7		
ν(C–C) asym	⎰ 1315.4		1319.1	1294.6
	⎱ 1297.3 sh			
ν(C–C) asym (II)			1285.3	1267.2
δ(CH) sym (II) ⎱			1266.4	⎰ 1252.0
ν(C–C) asym (III) ⎰				⎱ 1251.4
δ(CH) asym (III)			1234.1	1217.9
ν(C–O) sym		1226.2		1210.7
γ(CH$_3$) asym	1203.4		1199.7	1180.1
δ(CH) asym (II)			1177.2	1163.3
γ(CH$_3$) sym		1198.2		1171.9
δ(CH) asym	1164.8		1164.2	1147.9
γ(CH$_3$)' asym		⎰ 1162.8		1142.9
		⎱ 1142.4		
ν(C–O(CH$_3$)) asym (II) ⎱			1033.7	⎰ 1041.5
ν(C–O(CH$_3$)) asym (III) ⎰				⎱ 1036.7
ν(C–O(CH^3)) sym	⎰ 1016.2 sh		1020.8	996.0
	⎱ 1011.4			
γ(C–H) sym	998.4		986.0	999.7
γ(C–H) sym (III) ⎱			984.2	⎰ 1004.0
γ(C–H) sym (II) ⎰				⎱ 1002.6
ν(C–C) sym		964.1		951.3
ν(C–C) sym (II)			924.6	915.5
γ(C–H) asym		906.2		892.4
ν(C–O) asym	889.6		887.4	880.3
ν(C–O) asym (III)			863.4	864.5
ν(C–O) asym (II)			847.3	849.9
γ(C=O) sym (III) ⎱			800.6	⎰ 754.2
γ(C=O) asym (II) ⎰				⎱ 753.6
γ(C=O) sym	778.2		778.2	754.0
δ(C=O) sym		766.3		738.1
δ(C=O) sym (II)			748.5	735.6
δ(C=O) asym	674.6		672.2	660.3
δ(C=O) asym (III) ⎱			665.4	⎰ 656.4
δ(C=O) asym (II) ⎰				⎱ 652.9
δ(CCO) sym (II)			530.2	518.0
δ(CCO) asym	521.4		523.9	510.7
δ(COC) sym		400.6		359.8
δ(CC=C) sym		298.2		269.8
δ(CCO) sym		258.0		218.3
τ(C–O) asym		243.7		215.1
τ(CH$_3$) asym		139.5		115.5
τ(C–C) asym		106.4		102.6

[a] The bands ascribed to forms **II** and **III** in the spectrum of the amorphous layer are those that do not contain contributions from form **I**. Some of the bands assigned to form **I** may also have minor contributions from the other conformers.

Table 3 Theoretically calculated energies of the three conformers of dimethyl fumarate

	Relative energies/kJ mol^{-1}		
Conformer	**I** (C_{2h})	**II** (C_s)	**III** (C_{2h})
MP2/6-31G**	0.0	+3.42	+6.54
DFT(B3LYP)/6-31G**	0.0	+3.69	+6.48
ZPE(DFT)	0.0	−0.15	−0.07
Relative population[a] (%)	77.1	17.3	5.6

[a] Relative populations at 297 K.

stable conformer. Conformers **II** and **III** (C_{2h}) differ by nearly the same energy (3.1 kJ mol^{-1}; see Table 3). These results suggest that the energies of the stabilizing CH∴O=C weak hydrogen bond interactions are, to a fair approximation, additive. As already mentioned in the Introduction, such behaviour can be expected for DMFU, because the distance between the two ester groups is considerably large in this compound. A very similar relative conformational energy pattern has also been previously found for fumaric acid.[8]

The experimental IR spectrum of DMFU isolated in a Xe matrix is presented in Fig. 2(B). This spectrum is compared with that theoretically predicted (DFT(B3LYP)/6-31G**) for the most stable conformer **I**. From this comparison it is clear that the bands predicted for conformer **I** are present in the experimental spectrum. Apart from those, a number of additional bands were also observed experimentally. These bands indicate the presence of further conformational species in the matrix. Taking into consideration the results from the theoretical calculations, these species shall correspond to conformers **II** and **III**.

Upon annealing of the Xe matrix up to 60 K, significant changes occurred in the IR spectrum. The bands due to the most stable form **I** increased in intensity, while those due to forms **II** and **III** decreased (Fig. 3). This indicates the conversion of the two less stable conformers into the most stable form **I**. Because of the structural similarity of the three conformers, the IR spectra of all three forms are quite similar. However, there are enough spectral indications of the presence of both **II** and **III** conformers in the matrix after its deposition as will be pointed out in detail below.

It is important to note that all changes observed in the IR spectrum of DMFU during annealing concern relative changes in the intensities of three sets of bands already observable in the original spectrum that can be correlated with the three most stable conformers of the studied molecule. The fact that no new bands appear during annealing is a clear indication that the observed processes correspond to monomolecular conformational interconversions and not to any kind of associate formation.

Annealing of the Ar matrix was also carried out. However, annealing in Ar is possible only up to *ca.* 25 K and then the temperature needed to promote conformational interconversion processes is out of the available range (as mentioned above, in Xe these processes start to be clearly observed only at a temperature of *ca.* 60 K). Moreover, one can expect that, as is usually the case, the temperature needed to allow conformational interconversion in Ar matrixes should be higher than
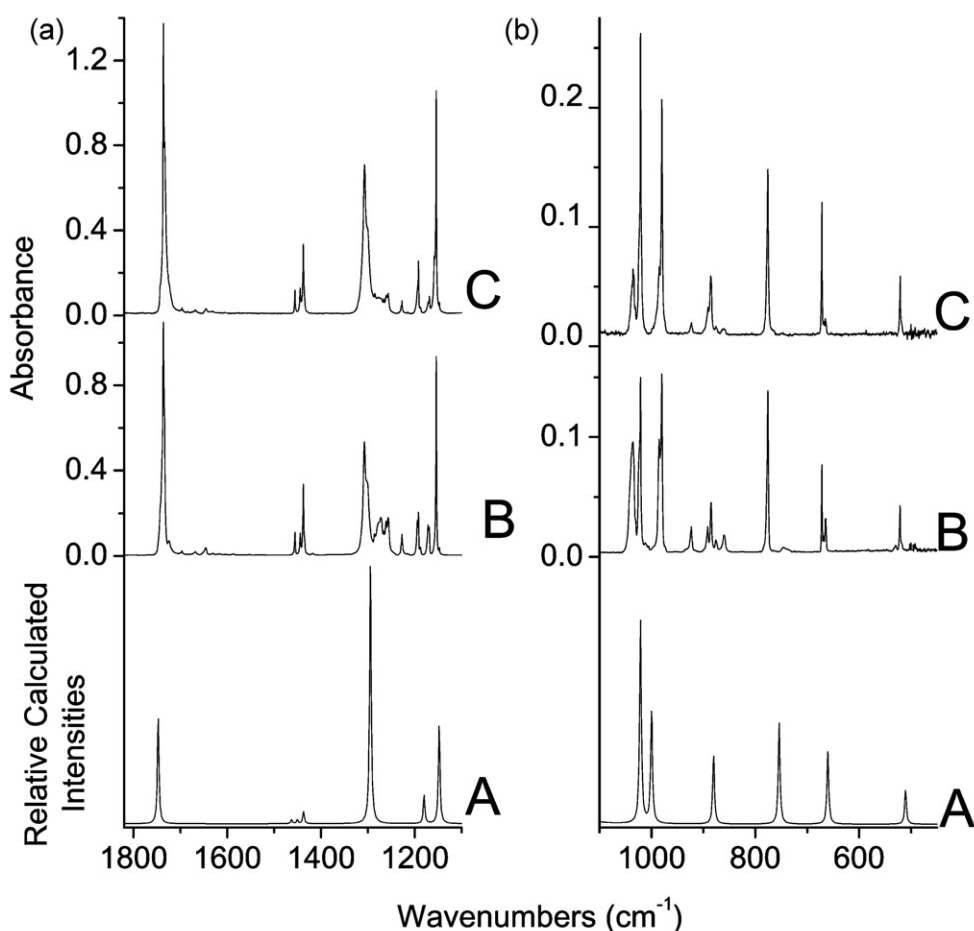
Fig. 2 Infrared spectra of DMFU: (A) calculated spectrum of conformer **I**; (B) experimental spectrum of the compound isolated in Xe matrix; (C) experimental spectrum of the compound after annealing of the matrix to 60 K. Theoretical spectra were calculated at the DFT(B3LYP)/6-31G** level and scaled down by a factor of 0.97. After annealing of the matrix to 60 K bands due to the less stable conformers **II** and **III** decreased in intensity, while the spectrum of conformer **I** correspondingly increased.
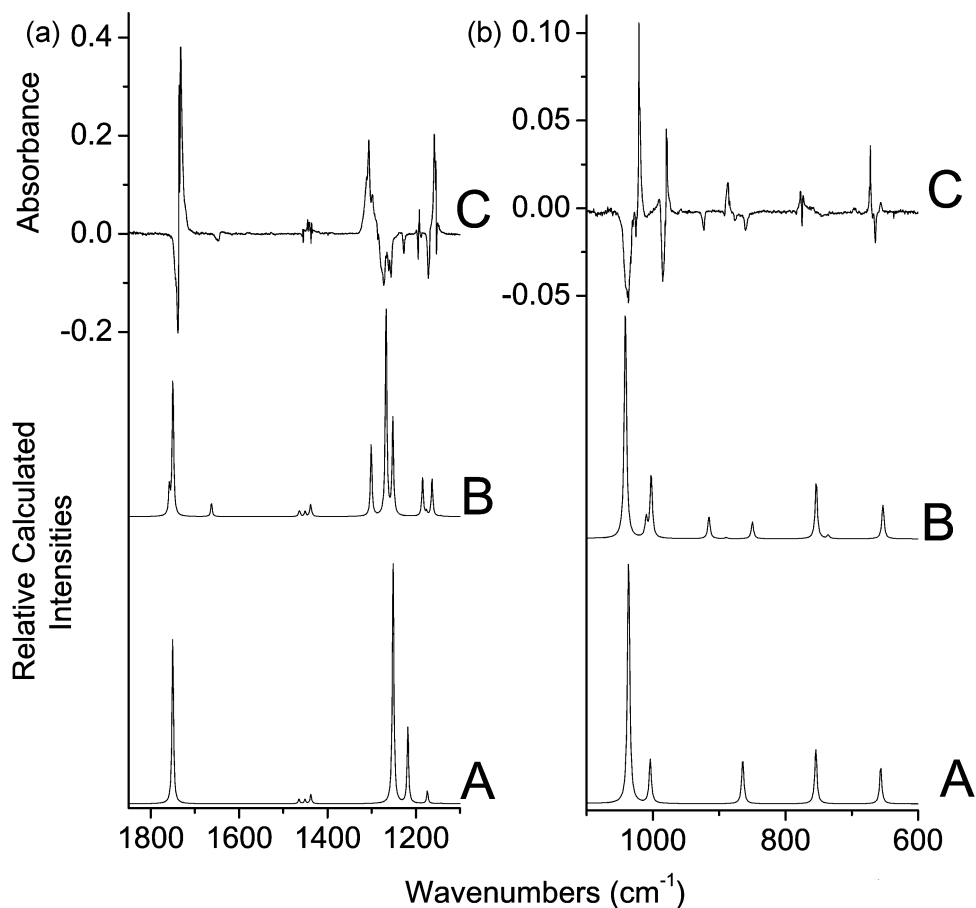
Fig. 3 Infrared spectra of DMFU in Xe matrix: (A) calculated spectrum of conformer **III**; (B) calculated spectrum of conformer **II**; (C) difference spectrum (spectrum at 60 K minus spectrum at 8 K). Theoretical spectra were calculated at the DFT(B3LYP)/6-31G** level and scaled down by a factor of 0.97. In the difference spectrum, peaks pointing down correspond to the bands that decrease after annealing (belonging to conformer **II** and conformer **III**). Peaks pointing up, which increase in intensity after annealing, are assigned to conformer **I**.

in Xe. The reason for that is the larger size of Xe atoms and, correspondingly, larger vacancy holes that allow easier intra-molecular rotation of the groups.

The spectrum of the most stable form **I** is much simplified because of the symmetry (C_{2h}) of this conformer. Having a center of symmetry, conformer **I** has only half of its vibrational modes active in the infrared and the assignment of these bands is straightforward (Table 1). On the other hand, conformer **II** is of C_s symmetry, so that all the modes are IR active. The bands at 1646, 923 and 745 in the spectra of DMFU in Xe (1653, 926 and 747 cm^{-1}, in Ar—see Table 1) are assigned to the ν(C=C), ν(C–C) sym and δ(C=O) sym vibrations of conformer **II**, that are predicted by the calculations at 1662, 916 and 736 cm^{-1}, respectively. These vibrations correspond to the modes (of symmetry A_g) non-active in the infrared, in both the most stable form **I** and conformer **III**. Their observation shows unequivocally that conformer **II** is present in the matrixes. Other bands observed in Xe matrix that originate exclusively in the conformer **II** are those at 530 (δ(CCO) sym), 665 (δ(C=O) asym), 860 (ν(C–O) asym), and 1195 cm^{-1} (γ(CH$_3$) asym) as well as the complex feature at 1169/1172/1174 (δ(CH) asym). All these bands follow the same pattern of variation of intensity upon annealing. Conformer **III** belongs to the same symmetry point group (C_{2h}) as conformer **I** and, as in the case of the later form, only half of its vibrations are infrared active. This makes the identification of the bands due to this form only by simple comparison of the experimental and calculated spectra more difficult. However, the pattern of variation of the intensities with temperature (during the annealing) of the bands due to this conformer is different from

that followed by the bands originating from conformer **II**. Indeed, by convenient spectra subtraction, bands due to form **III** could be removed from the experimental spectrum (see Fig. 4), enabling an unequivocal identification of the bands due to both higher energy forms. The bands observed at 669, 876 and 1227/1229 cm^{-1} in Xe (667, 876 and 1226/1229 cm^{-1}, in Ar), all of them following the same pattern of change of intensity upon annealing, confirm the presence of conformer **III** in the matrixes. These bands are ascribable to the δ(C=O) asym, ν(C–O) asym and δ(CH) asym vibrations, which calculated frequencies are 656, 864 and 1218 cm^{-1}, respectively. Some other bands due to forms **II** and **III** overlap in the experimental spectrum (see Table 1), though they appear at frequencies clearly different from the bands due to the dominant form **I**.

The fact that in the experimental spectra bands due to all individual conformers could be identified enabled the estimation of their relative populations in the matrixes. The bands originated in the δ(C=O) asym vibration are particularly useful for this purpose, since all three of them appear in a clean spectral region. From the relative intensities of the δ(C=O) asym bands observed in the spectrum of the freshly prepared Xe matrix, and taking into consideration the corresponding calculated intensities as normalizing factors, a **I**:**II**:**III** population ratio of 58:29:13% was determined. Assuming that no isomerization occurs during deposition, this population ratio should correspond to the population ratio of the compound in the vapour prior to deposition (297 K—nozzle temperature). The relative energies $\Delta H_{(II–I)}$ and $\Delta H_{(III–II)}$ can then be estimated, assuming the Boltzmann distribution as being *ca.* 2 kJ mol^{-1}.
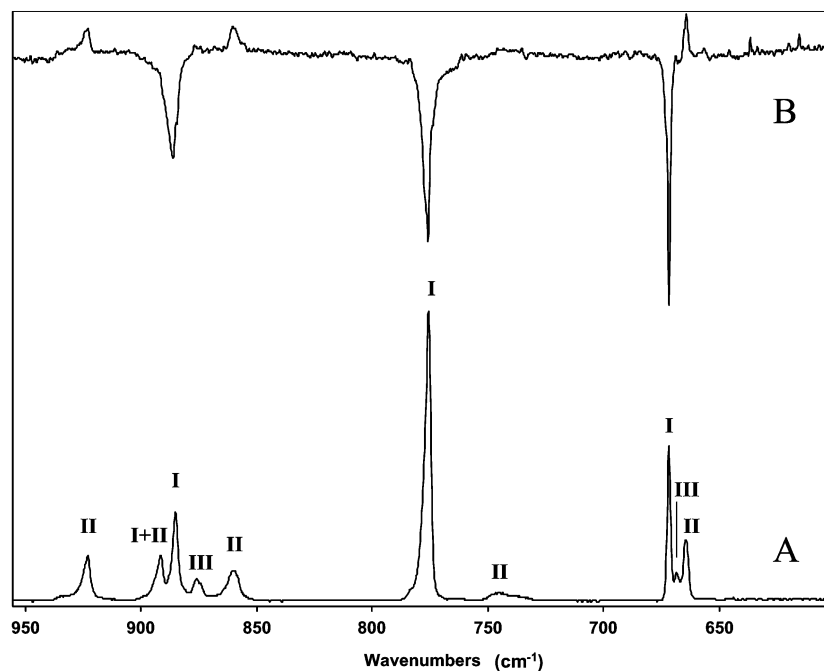
Fig. 4 Infrared spectra of DMFU in Xe matrix (600–950 cm^{-1} region): (A) reference experimental spectrum; (B) difference spectrum (spectrum at 8 K minus spectrum at 60 K) obtained using a subtraction factor selected to remove bands originated exclusively in conformer **III**. Peaks pointing down, which increase in intensity after annealing, are assigned to conformer **I**; peaks pointing up belong to conformer **II**.
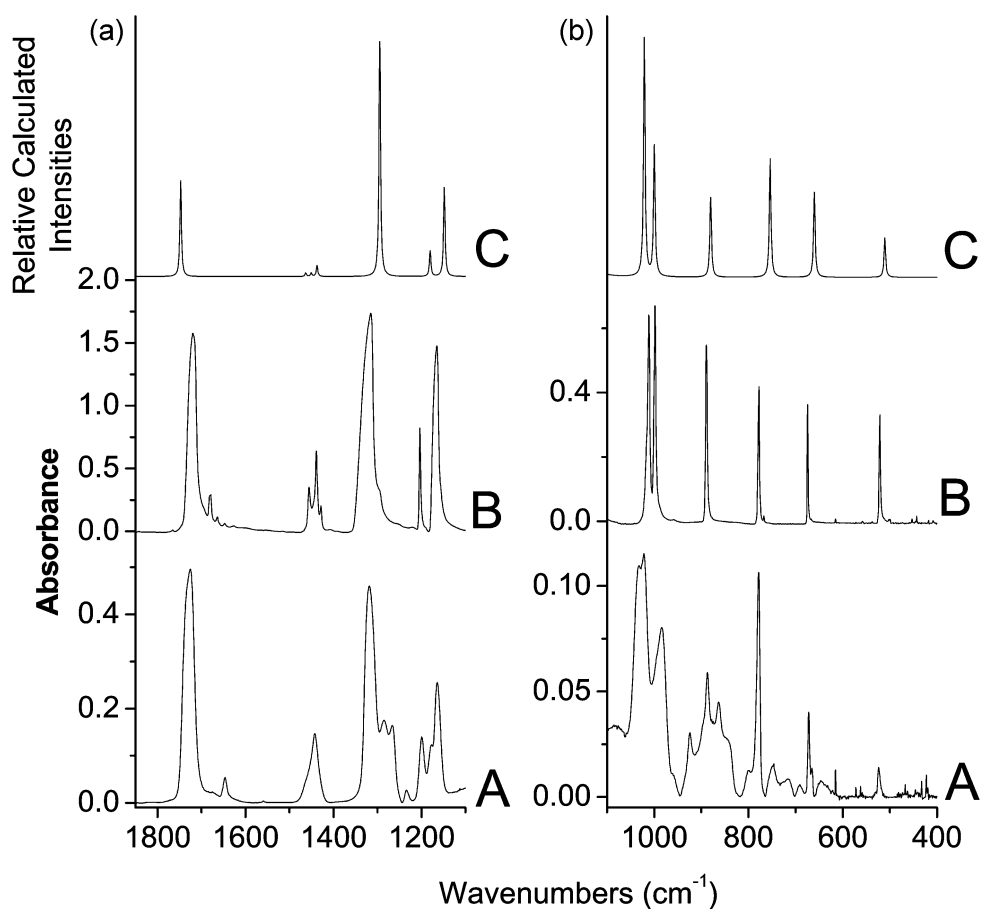
Fig. 5 Infrared spectra of solid DMFU: (A) amorphous, glassy layer of DMFU after deposition at 8 K; (B) after annealing to 200 K and cooling back to 8 K (crystal); (C) calculated spectrum of conformer **I**. After annealing of the amorphous layer to 160 K bands ascribed to conformers **II** and **III** disappeared while bands due to conformer **I** increased in intensity. Theoretical spectra were calculated at the DFT(B3LYP)/6-31G** level and scaled down by a factor of 0.97.

. This value compares fairly well with the theoretically predicted values (*ca.* 3 kJ mol^{-1}; see Table 3) and confirms the assumption of equal spacing of the conformational energy levels associated with the three observed conformers.

It is also worth noting that conformers **I** and **III** have dipole moments equal to zero, but conformer **II** has a markedly different dipole moment (3.42 D, in vacuum). This fact might, in principle, affect the conformer relative energies in the matrixes, since their solvation energies could be considerably different. However, calculation of the solvation energies for the three conformers of DMFU in Xe, undertaken within the frame of the polarized continuum model (PCM)[19] using the calculated gas phase structures and the dielectric constant of Xe (2.19),[20] enabled us to estimate the relative energies of the trapped conformers, resulting in relatively small changes with respect to the values obtained for the molecule in vacuum: $\Delta E_{II-I}(Xe) = 3.34$ kJ mol^{-1}; $\Delta E_{III-I}(Xe) = 6.16$ kJ mol^{-1}, which compare with 3.69 and 6.48 kJ mol^{-1}, respectively, for the molecule in vacuum (see also Table 3).

We have also carried out both UV ($\lambda > 250$ nm) and broad band IR *in situ* irradiation experiments. UV irradiation, using a standard xenon arc lamp as light source, was found to induce conversion of DMFU into its structural isomer, dimethyl maleate, together with some other unidentified photoproducts. The IR spectrum of matrix-isolated dimethyl maleate is extremely complex[21] and it obscures observation of other photoeffects. A similar UV ($\lambda = 266$ nm) photoisomerization of matrix-isolated fumaric acid to maleic acid was previously reported.[8] Also, as in the case of fumaric acid,[8] IR irradiation of DMFU matrixes was found to be inefficient in promoting any noticeable photochemical process. This result points to relatively large energy barriers for ground state isomerization for the matrix-isolated molecule, and is in agreement with the results of the annealing experiments. In addition, this result is also consistent with the previously estimated energy barrier for internal rotation about the C=C–C=O axis in acrylic acid, H$_2$C=CH–COOH, which amounts to 30.4 kJ mol^{-1}.[9]

The infrared spectra of the amorphous and crystalline layers of DMFU are shown in Fig. 5. As described in the Experimental section, the amorphous layer of the compound was prepared by deposition of vapours of DMFU directly onto the low temperature (8 K) KBr substrate of the cryostat. Under these experimental conditions it can be considered that the gas phase equilibrium population ratio of the three conformers can be efficiently frozen. It is clear that in the spectrum of the amorphous layer, infrared bands characteristic for each of the three conformers, **I**, **II** and **III**, are present. The presence of conformer **II** is unequivocally confirmed by the bands which appear at 1647, 1285, 925 and 847 cm^{-1}, assigned to the $\nu(C=C)$, $\nu(C-C)$ asym, $\nu(C-C)$ sym and $\nu(C-O)$ asym stretching modes, respectively, 1177 and 749 cm^{-1} which are mainly due to the δCH asym and $\delta(C=O)$ sym bending vibration, and the small band at 530 cm^{-1} ($\delta(CCO)$ sym). The corresponding predicted frequencies are 1662, 1267, 916, 850, 1163, 736 and 518 cm^{-1}, respectively (see Table 2). Form **III** gives rise to the bands at 1234 and 863 cm^{-1}, attributed to $\delta(CH)$ asym and $\nu(C-O)$ asym (calculated values: 1218 and 864 cm^{-1}). In addition, bands resulting from both conformers **II** and **III** are observed at 1266 cm^{-1} [overlapping bands due to $\delta(CH)$ sym of form **II** and $\nu(C-C)$ asym of form **III**, calculated values around 1250 cm^{-1}], 1034 cm^{-1} [$\nu(C-O(CH_3))$ asym, calculated values: 1042 and 1037 cm^{-1}], 984 cm^{-1} [$\gamma(CH)$ sym, calculated values: 1004 and 1003 cm^{-1}] and 665 cm^{-1} ($\delta(C=O)$ asym, calculated values: 653 and 656 cm^{-1}).

Increasing the temperature of the solid amorphous layer to 160 K led to the formation of well-organized crystals bound by weak CH∴O=C hydrogen bonds (the bands associated with the C=O vibration are visibly broader than the other bands in the spectrum of the crystal) and to the disappearance of the broader bands due to the less stable forms (con-
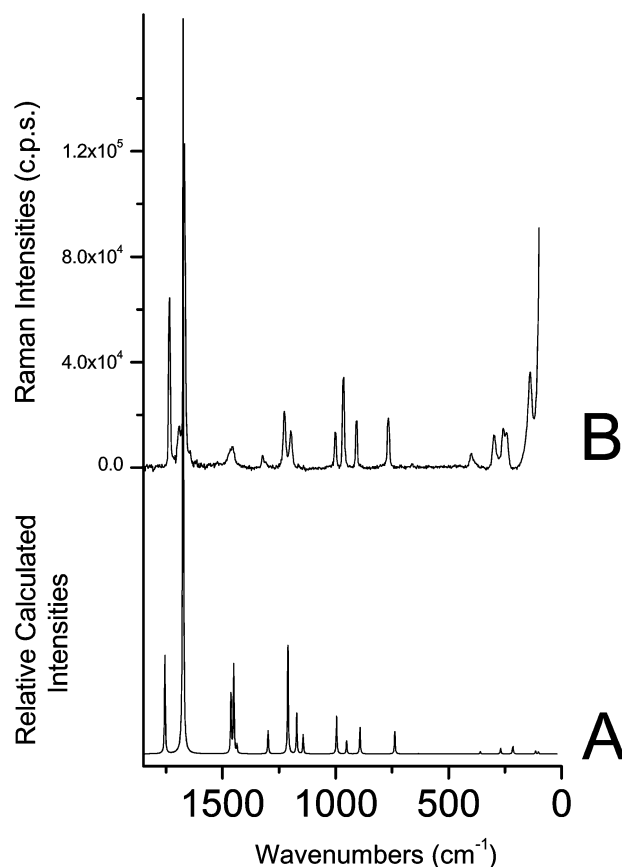

Fig. 6 Raman spectrum of crystalline DMFU: (A) calculated spectrum of conformer **I**; (B) experimentally observed Raman spectrum. The experimental Raman spectrum of the crystalline phase fits the theoretically predicted spectrum of conformer **I**. Theoretical spectra were calculated at the DFT(B3LYP)/6-31G** level and scaled down by a factor of 0.97.

formers **II** and **III**). The assignment of the bands in the infrared spectrum of the crystal is quite straightforward, since only bands ascribable to the lowest energy conformer **I** are present (see Fig. 5 and Table 2). Indeed, this spectrum is very well reproduced by the theoretically calculated spectrum for conformer **I**.

The Raman spectrum of crystalline DMFU (at room temperature) is shown in Fig. 6, where it may be compared with the calculated Raman spectrum for conformer **I**. The assignment of the bands in this spectrum (see Table 2) was also made without any particular difficulty, since the experimental data fits nicely the calculated spectrum. The experimental spectrum is not very complicated, because for conformer **I** only half of the normal modes are active in Raman scattering spectroscopy.

Conclusion

Dimethyl fumarate exists in the gas phase as a mixture of three conformers of low internal energy, all of them exhibiting the methyl ester moieties in the *cis* (C–O) configuration: the conformational ground state (conformer **I**), with the two O=C–C=C dihedral angles equal to 0°, and forms **II** and **III**, where one or both O=C–C=C dihedral angles are 180°. The conformational energy levels associated with these three forms were found to be nearly equally spaced by 2–3 kJ mol^{-1}. In the spectra of the matrix isolated compound (in Xe and Ar), characteristic bands of all three conformers were identified. Complete assignment of the spectra was undertaken for the first time. During annealing of the xenon matrix up to 60 K, conversion

of the less stable conformers, **II** and **III**, into the most stable conformer, **I**, was observed. In the amorphous solid, these three conformers could also be identified spectroscopically. On the other hand, IR and Raman spectra of the crystalline phase clearly show that only form **I** is present in the DMFU crystal.

Acknowledgements

References

1 N. A. Lange, *Handbook of Chemistry*, McGraw Hill, New York, 1961.
2 M. N. Islam, *J. Food Sci.*, 1982, **47**, 1710.
3 C. N. Huhtanen, *J. Food Sci.*, 1983, **48**, 1574.
4 M. N. Islam, F. R. Del Valle and L. Lirio, *J. Food Processing Preservation*, 1984, **8**, 41.
5 B. Sebok, B. Bonnekoh, R. Vetter, I. Schneider, H. Gollnick and G. Mahrle, *E. J. Derm.*, 1998, **8**(1), 29.
6 T. Otsu, T. Yasuhara and A. Matsumuto, *J. Macromol. Sci.-Chem., A*, 1988, **25**(5–7), 537.
7 S. Matsumara, H. Shigeno and T. Tanaka, *J. Am. Oil Chem. Soc.*, 1993, **7**, 659.
8 E. M. S. Maçôas, R. Fausto, J. Lundell, M. Pettersson, L. Khriachtchev and M. Rasanen, *J. Phys. Chem. A*, 2001, **105**, 3922.
9 A. Kulbida, M. N. Ramos, M. Rasanen, J. Nieminen, O. Schrems and R. Fausto, *J. Chem. Soc., Faraday Trans*, 1995, **91**(11), 1571.
10 R. Fausto, A. Kulbida and O. Schrems, *J. Chem. Soc., Faraday Trans.*, 1995, **91**(21), 3755.
11 M. D. G. Faria, J. J. C. Teixeira-Dias and R. Fausto, *Vib. Spectrosc.*, 1991, **2**, 43.
12 C. Téllez, R. Knudsen and O. Sala, *J. Mol. Struct.*, 1980, **67**, 189.
13 D. A. C. Compton, W. O. George and A. J. Porter, *J. Chem. Soc., Perkin Trans. II*, 1975, **71**, 400.
14 M. J. Frisch, G. W. Trucks, H. B. Schlegel, G. E. Scuseria, M. A. Robb, J. R. Cheeseman, V. G. Zakrzewski, J. A. Montgomery, Jr., R. E. Stratmann, J. C. Burant, S. Dapprich, J. M. Millam, A. D. Daniels, K. N. Kudin, M. C. Strain, O. Farkas, J. Tomasi, V. Barone, M. Cossi, R. Cammi, B. Mennucci, C. Pomelli, C. Adamo, S. Clifford, J. Ochterski, G. A. Petersson, P. Y. Ayala, Q. Cui, K. Morokuma, D. K. Malick, A. D. Rabuck, K. Raghavachari, J. B. Foresman, J. Cioslowski, J. V. Ortiz, A. G. Baboul, B. B. Stefanov, G. Liu, A. Liashenko, P. Piskorz, I. Komaromi, R. Gomperts, R. L. Martin, D. J. Fox, T. Keith, M. A. Al-Laham, C. Y. Peng, A. Nanayakkara, M. Challacombe, P. M. W. Gill, B. Johnson, W. Chen, M. W. Wong, J. L. Andres, C. Gonzalez, M. Head-Gordon, E. S. Replogle, and J. A. Pople, *Gaussian 98, Revision A.9*, Gaussian, Inc., Pittsburgh, PA, 1998.
15 J. H. Schachtschneider, *Technical Report*, Shell Development, Co, Emeryville, CA, 1969.
16 G. Keresztury and G. Jalsovszky, *J. Mol. Struct.*, 1971, **10**, 304.
17 L. A. E. Batista de Carvalho, J. J. C. Teixeira-Dias and R. Fausto, *THEOCHEM*, 1990, **208**, 109.
18 J. J. C. Teixeira-Dias, R. Fausto and L. A. E. Batista de Carvalho, *J. Comput. Chem.*, 1991, **12**, 1047.
19 S. Miertus, E. Scrocco and J. Tomasi, *Chem. Phys.*, 1981, **55**, 117.
20 H. E. Hallam and G. F. Scrimshaw, in *Vibrational Spectroscopy of Trapped Species*, ed. H. E. Hallam, John Wiley & Sons, London, 1973.
21 C. C. S. Silva, *Licenciaturship Thesis in Chemistry*, University of Coimbra, Portugal, 1999.